Macroscopic properties and field fluctuations in model power-law polycrystals: full-field solutions versus self-consistent estimates

By R. A. Lebensohn[1], Y. Liu[2] and P. Ponte Castañeda[2]

[1]Instituto de Física Rosario (UNR-CONICET), 2000 Rosario, Argentina
[2]Department of Mechanical Engineering and Applied Mechanics,
University of Pennsylvania, Philadelphia, PA 19104-6315, USA
(ponte@seas.upenn.edu)

This paper presents comparisons between full-field numerical results and homogenization estimates for the effective behaviour and statistical fluctuations of the stress and strain-rate fields in viscoplastic polycrystals. The full-field simulations make use of a recently introduced technique based on the fast Fourier transform (FFT) algorithm, while the homogenization results follow from the 'second-order' technique incorporating information about the averages and fluctuations of the fields in a suitably chosen 'linear comparison polycrystal', together with the standard self-consistent (SC) approximation for the linear comparison medium. An application is given for a model two-dimensional power-law polycrystal, for which exact estimates are available in the limit of linearly viscous behaviour. These exact results demonstrate the accuracy of the FFT method, even for relatively large values of the grain anisotropy parameter when the field fluctuations become significant. On the other hand, the 'second-order' SC estimates for both the effective behaviour and the statistical fluctuations of the stress and strain-rate fields in viscoplastic polycrystals are found to be in good agreement with the corresponding FFT results. This is the case even for strongly nonlinear systems with low strain-rate sensitivities, where the field fluctuations are found to be large, and where other, earlier versions of the SC approximation are shown to fail.

1. Introduction

Because macroscopic samples of most metals and minerals appear in polycrystalline form, the computation of the *effective* response of polycrystalline aggregates starting from the *properties* of their constituent single-crystal grains and *microstructure* is a fundamental problem in materials science. The simplest and perhaps most commonly used homogenization procedure in polycrystalline plasticity is the uniform strain-rate approximation of Taylor (1938). There is also the corresponding uniform-stress approximation of Reuss (1929). These two approximations have been shown (Hutchinson 1976) to provide rigorous upper and lower bounds, respectively, for the effective flow stress of viscoplastic polycrystals. Improved methods, based on various

types of ad hoc approximations, include several extensions of the self-consistent (SC) model, such as the 'incremental' method of Hill (1965) and Hutchinson (1976), and the 'tangent' procedure of Molinari *et al.* (1987) and Lebensohn & Tomé (1993). While these various approximations generally provide improvements on the Taylor and Reuss bounds, and reduce to the linear self-consistent estimate on which they are all based, for linearly viscous behaviour, they give widely diverging predictions for low-rate-sensitivity materials.

Alternative extensions of the SC estimates for viscoplastic polycrystals have been proposed recently making use of rigorous nonlinear homogenization methods (see Ponte Castañeda & Suquet (1998) for a recent review). More specifically, these novel SC estimates are based on the use of variational 'linear comparison' methods, which express the effective potential of the nonlinear viscoplastic polycrystal in terms of that of a linearly viscous polycrystal with properties that are determined from suitably designed variational principles. Two types of estimates are available depending on the method used. The first is based on the 'variational' method (Ponte Castañeda 1991; deBotton & Ponte Castañeda 1995), and makes use of the SC approximation for linearly viscous polycrystals to give bounds on the SC estimate for viscoplastic polycrystals (Ponte Castañeda & Nebozhyn 1997; Nebozhyn *et al.* 2001). The second is based on the recently proposed 'second-order' method (Ponte Castañeda 2002), and makes use of the SC approximation for a more general class of linearly viscous polycrystals to generate more accurate SC estimates for viscoplastic polycrystals (Liu & Ponte Castañeda 2004).

On the other hand, the dramatic increases in computational power in recent years have begun to make possible full-field simulations of polycrystalline samples. Pioneering contributions have been made by Beaudoin *et al.* (1995) and Balasubramanian & Anand (2002) using the finite-element method (FEM). Most of this work, however, has been concerned with texture predictions, and has used rather crude (one-element) discretizations of the constituent grains. Recently, an alternative technique based on the use of the fast Fourier transform (FFT) has been introduced by Moulinec & Suquet (1994, 1998). This technique has the advantage that it is amenable to finer discretization, and although it has mostly been used for composites thus far (Michel *et al.* 1999), applications of the method have been given recently for polycrystals (Lebensohn 2001; Suquet 2001; Bhattacharya & Suquet 2004).

The uncertainties associated with the various self-consistent schemes and the availability of powerful full-field numerical simulations suggest the use of the later to verify the accuracy of the former. In this paper, it is proposed to make use of the FFT technique, as generalized by Michel *et al.* (2000) and Lebensohn (2001), to carry out full-field simulations for a model, two-dimensional (2D) polycrystal, and to make comparisons with the corresponding SC predictions. The interest in this model problem derives from the fact that an *exact* estimate is available for its effective behaviour, and that the standard self-consistent model gives this estimate exactly, when the constitutive behaviour of the single crystals is taken to be *linear*. This allows a precise check on the accuracy of the full-field simulations, which will then be used as the reference standard to check the accuracy of the various SC models for more general nonlinear viscoplastic polycrystals, with the objective of discriminating among them. While the accuracy of a particular SC method for this special class of polycrystals will not prove its accuracy for more general classes of three-dimensional (3D) poly-

crystals, the failure of a given method for this special, but representative example, would severely compromise its validity for more general classes of polycrystals.

One of the advantages of the full-field FFT simulations is that they are not restricted to macroscopic predictions, and can be used to generate estimates for the local fields. On the other hand, the recently proposed 'second-order' method provides estimates not only for the macroscopic behaviour, but also for the statistical averages and fluctuations of the stress and strain fields within the grains of the polycrystal. Therefore, a second objective of this paper will be to investigate the heterogeneity of the stress and strain fields within the model polycrystal, as well as their dependence on material parameters such as the strain-rate sensitivity (nonlinearity) and grain anisotropy (heterogeneity contrast). This will be pursued here by means of both the FFT simulations and the 'second-order' method.

2. Theory

(a) Single-crystal behaviour and macroscopic properties of the polycrystal

For the purposes of this work, *polycrystals* will be taken to be random aggregates of perfectly bonded single-crystal grains with varying orientations. Furthermore, the distribution of the grains in the polycrystals will be taken to be statistically homogenous, so that the standard ergodic hypothesis will allow the replacement of ensemble averages by volume averages over a suitably defined *representative volume element* (RVE) of the polycrystal. An orientation distribution function (ODF) may then be defined (see Adams & Olson 1998), serving to characterize the *crystallographic texture* of the polycrystal. For simplicity, it will be assumed here that the grain orientations take on a set of discrete values, defined by rotation tensors $\boldsymbol{Q}^{(r)}$ ($r = 1, \ldots, N$). The RVE of the polycrystal is assumed to occupy a domain Ω, while all the grains of a given orientation $\boldsymbol{Q}^{(r)}$ occupy 'phases' $\Omega^{(r)}$ ($r = 1, \ldots, N$), such that

$$\Omega = \bigcup_{r=1}^{N} \Omega^{(r)}.$$

The characteristic functions $\chi^{(r)}$ describing the location of the various orientations are defined to be equal to unity if the position vector $\boldsymbol{x}$ is in $\Omega^{(r)}$ and zero otherwise. Volume averages over Ω are denoted by $\langle \cdot \rangle$, so that the scalars $c^{(r)} = \langle \chi^{(r)} \rangle$ characterize the crystallographic texture of the polycrystal. Similarly, volume averages over the phases $\Omega^{(r)}$ will be denoted $\langle \cdot \rangle^{(r)}$.

Now, for a given stress $\boldsymbol{\sigma}$, the *local* constitutive response is defined by

$$\boldsymbol{\varepsilon} = \frac{\partial u}{\partial \boldsymbol{\sigma}}, \quad u(\boldsymbol{x}, \boldsymbol{\sigma}) = \sum_{r=1}^{N} \chi^{(r)}(\boldsymbol{x}) u^{(r)}(\boldsymbol{\sigma}), \quad u^{(r)}(\boldsymbol{\sigma}) = \sum_{k=1}^{K} \phi_{(k)}^{(r)}(\tau_{(k)}^{(r)}), \qquad (2.1)$$

where $\boldsymbol{\varepsilon}$ is the Eulerian strain rate, and u and $u^{(r)}$ are the stress potentials for the polycrystal and a single crystal with orientation $\boldsymbol{Q}^{(r)}$, respectively. The convex functions $\phi_{(k)}^{(r)}$ ($k = 1, \ldots, K$) characterize the response of the K slip systems in a crystal with orientation $\boldsymbol{Q}^{(r)}$ and depend on the resolved shear (or Schmid) stresses

$$\tau_{(k)}^{(r)} = \boldsymbol{\sigma} \cdot \boldsymbol{\mu}_{(k)}^{(r)}, \quad \boldsymbol{\mu}_{(k)}^{(r)} = \tfrac{1}{2}(\boldsymbol{n}_{(k)}^{(r)} \otimes \boldsymbol{m}_{(k)}^{(r)} + \boldsymbol{m}_{(k)}^{(r)} \otimes \boldsymbol{n}_{(k)}^{(r)}). \qquad (2.2)$$

Here the $\boldsymbol{\mu}_{(k)}^{(r)}$ are second-order tensors with $\boldsymbol{n}_{(k)}^{(r)}$ and $\boldsymbol{m}_{(k)}^{(r)}$ denoting the unit vectors normal to the slip plane and along the slip direction of the kth system, respectively, for a crystal with orientation $\boldsymbol{Q}^{(r)}$. Note that the Schmid tensors $\boldsymbol{\mu}_{(k)}^{(r)}$ for a one-phase polycrystal are related to corresponding tensors $\boldsymbol{\mu}_{(k)}$ for a 'reference' crystal via

$$\boldsymbol{\mu}_{(k)}^{(r)} = \boldsymbol{Q}^{(r)\mathrm{T}} \boldsymbol{\mu}_{(k)} \boldsymbol{Q}^{(r)}.$$

In this work dealing with polycrystals made up of only one type of single crystal, the slip potentials of the grains with various orientations will be taken to be the same, i.e. $\phi_{(k)}^{(r)} = \phi_{(k)}$. Furthermore, for simplicity, use will be made here of the standard power-law choice for these slip potentials:

$$\phi_{(k)}(\tau) = \frac{\gamma_0(\tau_0)_{(k)}}{n+1} \left| \frac{\tau}{(\tau_0)_{(k)}} \right|^{n+1}, \tag{2.3}$$

where $m = 1/n$ ($0 \leqslant m \leqslant 1$) is the strain-rate sensitivity, $(\tau_0)_{(k)} > 0$ is the reference flow stress of the kth slip system, and γ_0 is a reference shear rate. Note that the limit as the nonlinearity parameter (n) tends to infinity is of special interest, as it corresponds to rigid ideally plastic behaviour.

For the class of viscoplastic polycrystals whose local constitutive behaviour is given by (2.1) and (2.2), it is known (e.g. Ponte Castañeda & Suquet 1998) that the *effective* response for the polycrystal, characterizing the relation between the *average* strain rate $\boldsymbol{E} = \langle \boldsymbol{\varepsilon} \rangle$ and stress $\boldsymbol{\Sigma} = \langle \boldsymbol{\sigma} \rangle$, is given by

$$\boldsymbol{E} = \frac{\partial \tilde{U}}{\partial \boldsymbol{\Sigma}}, \quad \tilde{U}(\boldsymbol{\Sigma}) = \min_{\boldsymbol{\sigma} \in \mathcal{S}(\boldsymbol{\Sigma})} \langle u(\boldsymbol{x}, \boldsymbol{\sigma}) \rangle = \min_{\boldsymbol{\sigma} \in \mathcal{S}(\boldsymbol{\Sigma})} \sum_{r=1}^{N} c^{(r)} \langle u^{(r)}(\boldsymbol{\sigma}) \rangle^{(r)}. \tag{2.4}$$

Here, $\tilde{U}$ is the *effective stress potential* for the polycrystal, and

$$\mathcal{S}(\boldsymbol{\Sigma}) = \{ \boldsymbol{\sigma}, \text{such that div } \boldsymbol{\sigma} = \boldsymbol{0} \text{ and } \langle \boldsymbol{\sigma} \rangle = \boldsymbol{\Sigma} \text{ in } \Omega \}$$

defines the set of statically admissible stresses.

(b) The 'second-order' homogenization theory

In this subsection, the 'second-order' homogenization method (Liu & Ponte Castañeda 2004) for viscoplastic polycrystals is recalled, which is a generalization of the method proposed by Ponte Castañeda (2002) for nonlinear composite materials. In turn, these formulations constitute improvements on an earlier version of the method (Ponte Castañeda 1996), which neglected the field fluctuations, but which also led to estimates that are exact to second order in the heterogeneity contrast (Suquet & Ponte Castañeda 1993).

(i) The linear comparison polycrystal

The key idea of the 'second-order' method is to introduce a 'linear thermoelastic comparison polycrystal' with local and grain-level stress potentials given by

$$u_{\mathrm{T}}(\boldsymbol{x}, \boldsymbol{\sigma}) = \sum_{r=1}^{N} \chi^{(r)}(\boldsymbol{x}) u_{\mathrm{T}}^{(r)}(\boldsymbol{\sigma}), \qquad u_{\mathrm{T}}^{(r)}(\boldsymbol{\sigma}) = \tfrac{1}{2} \boldsymbol{\sigma} \cdot \boldsymbol{M}^{(r)} \boldsymbol{\sigma} + \boldsymbol{e}^{(r)} \cdot \boldsymbol{\sigma}, \tag{2.5}$$

where

$$\boldsymbol{M}^{(r)} = \sum_{k=1}^{K} \alpha_{(k)}^{(r)} \boldsymbol{\mu}_{(k)}^{(r)} \otimes \boldsymbol{\mu}_{(k)}^{(r)} \quad \text{and} \quad \boldsymbol{e}^{(r)} = \sum_{k=1}^{K} e_{(k)}^{(r)} \boldsymbol{\mu}_{(k)}^{(r)} \tag{2.6}$$

define the viscous-compliance and 'residual' strain-rate tensors at the grain level in terms of the corresponding slip-level quantities $\alpha_{(k)}^{(r)}$ and $e_{(k)}^{(r)}$, respectively.

The effective behaviour of this linear comparison polycrystal is characterized by a stress potential $\tilde{U}_{\mathrm{T}}$ defined by

$$\tilde{U}_{\mathrm{T}}(\boldsymbol{\Sigma}) = \min_{\boldsymbol{\sigma} \in \mathcal{S}(\boldsymbol{\Sigma})} \langle u_{\mathrm{T}}(\boldsymbol{x}, \boldsymbol{\sigma}) \rangle = \min_{\boldsymbol{\sigma} \in \mathcal{S}(\boldsymbol{\Sigma})} \sum_{r=1}^{N} c^{(r)} \langle \tfrac{1}{2} \boldsymbol{\sigma} \cdot \boldsymbol{M}^{(r)} \boldsymbol{\sigma} + \boldsymbol{e}^{(r)} \cdot \boldsymbol{\sigma} \rangle^{(r)}. \tag{2.7}$$

Because of the linearity of the problem, it is known (Laws 1973) that the average of the stress over phase r in this linear comparison 'thermoelastic' composite may be written in the form:

$$\bar{\boldsymbol{\sigma}}^{(r)} = \boldsymbol{B}^{(r)} \boldsymbol{\Sigma} + \boldsymbol{b}^{(r)}, \tag{2.8}$$

where $\boldsymbol{B}^{(r)}$ and $\boldsymbol{b}^{(r)}$ are concentration tensors depending on the homogenization procedure used. Using these concentration tensors, the effective potential $\tilde{U}_{\mathrm{T}}$ may be written (Laws 1973; Willis 1981) in the form:

$$\tilde{U}_{\mathrm{T}}(\boldsymbol{\Sigma}) = \tfrac{1}{2} \boldsymbol{\Sigma} \cdot \tilde{\boldsymbol{M}} \boldsymbol{\Sigma} + \tilde{\boldsymbol{e}} \cdot \boldsymbol{\Sigma} + \tfrac{1}{2} \tilde{g}, \tag{2.9}$$

such that the associated effective stress–strain-rate relation is given by

$$\boldsymbol{E} = \tilde{\boldsymbol{M}} \boldsymbol{\Sigma} + \tilde{\boldsymbol{e}}, \tag{2.10}$$

where

$$\tilde{\boldsymbol{M}} = \sum_{r=1}^{N} c^{(r)} \boldsymbol{M}^{(r)} \boldsymbol{B}^{(r)}, \qquad \tilde{\boldsymbol{e}} = \sum_{r=1}^{N} c^{(r)} \boldsymbol{e}^{(r)} \boldsymbol{B}^{(r)}, \qquad \tilde{g} = \sum_{r=1}^{N} c^{(r)} \boldsymbol{e}^{(r)} \cdot \boldsymbol{b}^{(r)} \tag{2.11}$$

are the effective compliance, effective residual strain rate and effective energy under zero applied stress, respectively.

Therefore, given explicit estimates for the concentration tensors $\boldsymbol{B}^{(r)}$ and $\boldsymbol{b}^{(r)}$ (see further below), corresponding estimates may be generated for the phase averages $\bar{\boldsymbol{\sigma}}^{(r)}$ and the effective potential $\tilde{U}_{\mathrm{T}}$ of the linear comparison polycrystal. In addition, estimates for the second moments of the stress over phase r may be obtained from

$$\langle \boldsymbol{\sigma} \otimes \boldsymbol{\sigma} \rangle^{(r)} = \frac{2}{c^{(r)}} \frac{\partial \tilde{U}_{\mathrm{T}}}{\partial \boldsymbol{M}^{(r)}}, \tag{2.12}$$

where the variables $\boldsymbol{e}^{(r)}$ are held fixed in the differentiation. Corresponding expressions may then be generated for the phase fluctuation covariance tensors

$$\boldsymbol{C}_{\boldsymbol{\sigma}}^{(r)} \doteq \langle (\boldsymbol{\sigma} - \bar{\boldsymbol{\sigma}}^{(r)}) \otimes (\boldsymbol{\sigma} - \bar{\boldsymbol{\sigma}}^{(r)}) \rangle^{(r)} = \langle \boldsymbol{\sigma} \otimes \boldsymbol{\sigma} \rangle^{(r)} - \bar{\boldsymbol{\sigma}}^{(r)} \otimes \bar{\boldsymbol{\sigma}}^{(r)}. \tag{2.13}$$

Self-consistent estimates for thermoelastic systems are available from Laws (1973) and Willis (1981). Expressions for the relevant concentration tensors are given by

$$\boldsymbol{B}^{(r)} = [\boldsymbol{M}^{(r)} + \tilde{\boldsymbol{M}}^{\star}]^{-1} \tilde{\boldsymbol{Q}}^{-1} \quad \text{and} \quad \boldsymbol{b}^{(r)} = [\boldsymbol{M}^{(r)} + \tilde{\boldsymbol{M}}^{\star}]^{-1} [\tilde{\boldsymbol{e}} - \boldsymbol{e}^{(r)}]. \tag{2.14}$$

In these relations, $\tilde{\boldsymbol{M}}^{\star} = \tilde{\boldsymbol{Q}}^{-1} - \tilde{\boldsymbol{M}}$ is the constraint tensor defined by Hill (1965), where $\tilde{\boldsymbol{M}}$ is the self-consistent estimate for the effective modulus tensor which is obtained as the solution of the implicit equation

$$[\tilde{\boldsymbol{M}} + \tilde{\boldsymbol{M}}^{\star}]^{-1} = \sum_{s=1}^{N} c^{(s)} [\boldsymbol{M}^{(s)} + \tilde{\boldsymbol{M}}^{\star}]^{-1}, \qquad (2.15)$$

also involving $\tilde{\boldsymbol{M}}^{\star}$, and $\tilde{\boldsymbol{Q}}$ is a microstructural tensor, depending on $\tilde{\boldsymbol{M}}$ and on the 'shape' of the two-point correlation functions $\langle \chi^{(r)} \chi^{(s)} \rangle$ for the distribution of the grain orientations within the polycrystal. The tensor $\tilde{\boldsymbol{Q}}$ may be expressed in terms of a closely related tensor $\tilde{\boldsymbol{P}}$ via $\tilde{\boldsymbol{Q}} = \tilde{\boldsymbol{L}} - \tilde{\boldsymbol{L}}\tilde{\boldsymbol{P}}\tilde{\boldsymbol{L}}$, where $\tilde{\boldsymbol{P}}$ is given by

$$\tilde{\boldsymbol{P}} = \frac{1}{4\pi \det \boldsymbol{Z}} \int_{|\boldsymbol{\xi}|=1} \tilde{\boldsymbol{H}}(\boldsymbol{\xi}) |\boldsymbol{Z}^{-1}\boldsymbol{\xi}|^{-3} \, \mathrm{d}S. \qquad (2.16)$$

Here, $\tilde{H}_{ijkh}(\boldsymbol{\xi}) = \tilde{N}_{ik}\xi_j\xi_h|_{(ij)(kh)}$, $\tilde{\boldsymbol{N}} = \tilde{\boldsymbol{K}}^{-1}$, $\tilde{K}_{ik} = \tilde{L}_{ijkh}\xi_j\xi_h$ and $\boldsymbol{Z}$ is a symmetric, second-order tensor serving to characterize the 'shape' of the two-point correlation functions, under the 'ellipsoidal symmetry' hypothesis (Willis 1977). For a polycrystal, the shape of the two-point correlation functions is known to correlate with the 'average' shape of the grains. In particular, $\boldsymbol{Z} = \boldsymbol{I}$ corresponds to the special case of statistical isotropy for the two-point correlation functions, which is equivalent to the hypothesis of 'equi-axed' grains.

(ii) *The nonlinear polycrystal*

By approximating the local potential of the nonlinear polycrystal u in terms of the local potential of the above-defined linear comparison polycrystal u_{T} and a suitable measure of the error, Liu & Ponte Castañeda (2004) generated the following approximation for the effective potential of the nonlinear polycrystal:

$$\tilde{U}(\boldsymbol{\Sigma}) = \sum_{r=1}^{N} \sum_{k=1}^{K} c^{(r)} \{ \phi_{(k)}^{(r)}(\hat{\tau}_{(k)}^{(r)}) + \phi_{(k)}^{(r)\prime}(\bar{\tau}_{(k)}^{(r)})(\bar{\tau}_{(k)}^{(r)} - \hat{\tau}_{(k)}^{(r)}) \} \quad \text{(energy)}, \qquad (2.17)$$

where the variables

$$\bar{\tau}_{(k)}^{(r)} \quad \text{and} \quad \hat{\tau}_{(k)}^{(r)}$$

depend on the averages and fluctuations of the resolved shear stress $\tau_{(k)}^{(r)}$ on the slip systems k for grain orientations r in the linear comparison polycrystal, defined by relations (2.5) and (2.6), in such a way that

$$\bar{\tau}_{(k)}^{(r)} \doteq \langle \tau_{(k)}^{(r)} \rangle^{(r)} = \bar{\boldsymbol{\sigma}}^{(r)} \cdot \boldsymbol{\mu}_{(k)}^{(r)}, \qquad (2.18)$$

and

$$(\hat{\tau}_{(k)}^{(r)} - \bar{\tau}_{(k)}^{(r)})^2 \doteq \langle (\tau_{(k)}^{(r)} - \bar{\tau}_{(k)}^{(r)})^2 \rangle^{(r)} = \boldsymbol{\mu}_{(k)}^{(r)} \cdot \boldsymbol{C}_{\sigma}^{(r)} \boldsymbol{\mu}_{(k)}^{(r)}, \qquad (2.19)$$

where the quantities $\hat{\tau}_{(k)}^{(r)} - \bar{\tau}_{(k)}^{(r)}$ are taken to have the same sign as the $\bar{\tau}_{(k)}^{(r)}$.

In turn, the linear comparison polycrystal must be chosen such that the variables $e_{(k)}^{(r)}$ and $\alpha_{(k)}^{(r)}$ introduced in the context of relations (2.6) for $\boldsymbol{e}^{(r)}$ and $\boldsymbol{M}^{(r)}$ satisfy the relations

$$e_{(k)}^{(r)} = \phi_{(k)}^{(r)\prime}(\bar{\tau}_{(k)}^{(r)}) - \alpha_{(k)}^{(r)}\bar{\tau}_{(k)}^{(r)}, \qquad (2.20)$$

and

$$\phi_{(k)}^{(r)\prime}(\hat{\tau}_{(k)}^{(r)}) - \phi_{(k)}^{(r)\prime}(\bar{\tau}_{(k)}^{(r)}) = \alpha_{(k)}^{(r)}(\hat{\tau}_{(k)}^{(r)} - \bar{\tau}_{(k)}^{(r)}). \tag{2.21}$$

Note that equation (2.21) identifies the viscous slip compliances $\alpha_{(k)}^{(r)}$ of the linear comparison polycrystal with a 'generalized secant' approximation of the nonlinear constitutive relation for the corresponding slip systems in the viscoplastic polycrystal, taking into account both the average and fluctuation of the stress for the given grain orientation (as determined by the linear comparison approximation). Note also that the variables $\bar{\tau}_{(k)}^{(r)}$ and $\hat{\tau}_{(k)}^{(r)}$ appearing in expression (2.17) for $\tilde{U}$ can be computed making use of the self-consistent estimates (2.14) for the concentration tensors $\boldsymbol{B}^{(r)}$ and $\boldsymbol{b}^{(r)}$.

Moreover, it is known (Liu & Ponte Castañeda 2004) that the effective stress–strain-rate relation for the nonlinear polycrystal, obtained from relation $(2.4)_1$ and expression (2.17) for $\tilde{U}$, does not coincide with the effective stress–strain-rate relation (2.10) for the linear comparison polycrystal, when use is made of (2.20) and (2.21) to specify the linear comparison composite. In fact, an *alternate* version of the 'second-order' theory may be generated by making use of the effective stress–strain-rate relations for the linear comparison polycrystal. The resulting estimate for the nonlinear polycrystal can be shown to reduce to

$$\boldsymbol{E} = \sum_{r=1}^{N}\sum_{k=1}^{K} c^{(r)} \phi_{(k)}^{(r)\prime}(\bar{\tau}_{(k)}^{(r)}) \boldsymbol{\mu}_{(k)}^{(r)} \quad \text{(constitutive relation)}. \tag{2.22}$$

This estimate has the advantage of greater simplicity, but the disadvantage that it does not possess an associated potential function $\tilde{U}$, and that is not exact to second order in the heterogeneity contrast. It can be interpreted as generalization of the so-called 'affine' approximation of Masson *et al.* (2000).

A consequence of the comments in the preceding paragraph is the existence of a duality gap in the theory (see Ponte Castañeda (2002) for more details). However, in general, it is still useful to have consistent expressions for the average slip rates, and their fluctuations. Thus, using certain *restricted* duality conditions, Liu & Ponte Castañeda (2004) demonstrated that the following relations are satisfied:

$$\bar{\gamma}_{(k)}^{(r)} = \phi_{(k)}^{(r)\prime}(\bar{\tau}_{(k)}^{(r)}) \quad \text{and} \quad \hat{\gamma}_{(k)}^{(r)} = \phi_{(k)}^{(r)\prime}(\hat{\tau}_{(k)}^{(r)}), \tag{2.23}$$

where the $\bar{\gamma}_{(k)}^{(r)}$ and the $\hat{\gamma}_{(k)}^{(r)}$ are consistent with relations

$$\bar{\boldsymbol{\varepsilon}}^{(r)} = \sum_{k=1}^{K} \bar{\gamma}_{(k)}^{(r)} \boldsymbol{\mu}_{(k)}^{(r)} \qquad \boldsymbol{L}^{(r)} \cdot \boldsymbol{C}_{\boldsymbol{\varepsilon}}^{(r)} = \sum_{k=1}^{K} \frac{1}{\alpha_{(k)}^{(r)}}(\hat{\gamma}_{(k)}^{(r)} - \bar{\gamma}_{(k)}^{(r)})^2, \tag{2.24}$$

with

$$\boldsymbol{L}^{(r)} = (\boldsymbol{M}^{(r)})^{-1}, \qquad \boldsymbol{C}_{\boldsymbol{\varepsilon}}^{(r)} = \langle (\boldsymbol{\varepsilon} - \bar{\boldsymbol{\varepsilon}}^{(r)}) \otimes (\boldsymbol{\varepsilon} - \bar{\boldsymbol{\varepsilon}}^{(r)}) \rangle^{(r)}.$$

Note, however, that the expressions

$$\bar{\gamma}_{(k)}^{(r)} = 2\bar{\boldsymbol{\varepsilon}}^{(r)} \cdot \boldsymbol{\mu}_{(k)}^{(r)}, \qquad (\hat{\gamma}_{(k)}^{(r)} - \bar{\gamma}_{(k)}^{(r)})^2 = \langle [2(\boldsymbol{\varepsilon} - \bar{\boldsymbol{\varepsilon}}^{(r)}) \cdot \boldsymbol{\mu}_{(k)}^{(r)}]^2 \rangle^{(r)},$$

are valid only when the $\boldsymbol{\mu}_{(k)}^{(r)}$ are orthogonal for a given orientation r.

(c) The FFT approach

Moulinec & Suquet (1994, 1998) developed an iterative method based on the FFT algorithm to compute the effective properties and local response of elastic and elastoplastic composites consisting of two isotropic phases with different properties. The Moulinec–Suquet FFT formulation is conceived for periodic heterogeneous microstructures, provides an exact solution of the governing equations and has better numerical performance than a standard FEM calculation for the same purpose. Lebensohn (2001) adapted the Moulinec–Suquet FFT formulation to compute local fields and to predict overall and local texture development in viscoplastic anisotropic 3D polycrystals. However, as discussed by Michel *et al.* (1999), and shown by Lebensohn (2001), the applicability of the iterative method to materials with low rate sensitivity (highly nonlinear) and strongly anisotropic properties is limited to a few initial iterations, after which the convergence towards the fulfilment of equilibrium starts to deteriorate. To overcome this limitation, Michel *et al.* (2000) proposed an improved FFT formulation for isotropic composites with high contrast of the properties between phases, based on an augmented Lagrangian method. In the present work, the formulation of Michel *et al.* (2000) has been successfully adapted to deal with anisotropic power-law polycrystals. Briefly, the improved FFT formulation consists in finding a strain-rate field, associated with a kinematically admissible velocity field, that minimizes the average of the local strain energies, under the constraint imposed by the strain compatibility condition (see Michel *et al.* (2000) for details). The general features of this improved method are the following.

(i) *Discretization.* The FFT method is based on the solution of a unit-cell problem with periodic boundary conditions. For numerical purposes, in order to apply the discrete Fourier transform, the unit cell under consideration should be discretized into $N_1 \times N_2$ (in two dimensions) or $N_1 \times N_2 \times N_3$ Fourier points (in three dimensions). This discretization determines a regular grid in the Cartesian space $\{x_d\}$ and a corresponding grid in the Fourier space $\{\xi_d\}$.

(ii) *Linear reference medium.* The method requires the selection of a linear reference medium of stiffness L^0. The choice made for L^0 can be quite general, but the convergence of the method will depend on this choice. Then, for each point of the grid in the Fourier space $\xi \in \{\xi_d\}$, the Fourier transform of the viscoplastic Green operator $\Gamma^0(\xi)$ associated with L^0 is obtained (see Moulinec & Suquet (1998) for the definition of Γ^0, and Lebensohn (2001) for details of the calculation of Γ^0 in viscoplasticity).

Once the discretization and the linear reference medium have been chosen, the implementation of the FFT-based algorithm, for power-law polycrystals whose local constitutive behaviour is given by equations (2.1)–(2.3), consists of the following steps.

(i) Initialization

If a macroscopic strain rate E is imposed on the unit cell, the algorithm can be initialized under a uniform strain-rate assumption: $\breve{\varepsilon}^0(x) = 0 \; \forall x \in \{x_d\}$, where $\breve{\varepsilon}^0(x)$ is the initial guess for the local strain-rate deviation field, i.e. $\breve{\varepsilon}(x) = \varepsilon(x) - E$. Next, the initial guess of the stress field $\sigma^0(x)$ is obtained from the local constitutive relation given by equations (2.1)–(2.3), $\forall x \in \{x_d\}$. Furthermore, it can be assumed that

$\boldsymbol{\lambda}^0(\boldsymbol{x}) = \boldsymbol{\sigma}^0(\boldsymbol{x})$, where $\boldsymbol{\lambda}^0(\boldsymbol{x})$ is the initial guess for the field of Lagrange multipliers associated with the compatibility constraint.

(ii) *Iterative procedure*

If $\breve{\boldsymbol{\varepsilon}}^i(\boldsymbol{x})$ and $\boldsymbol{\lambda}^i(\boldsymbol{x})$ are known $\forall \boldsymbol{x} \in \{\boldsymbol{x}_\mathrm{d}\}$, the $(i+1)$th iteration starts with the calculation of the polarization field: $\boldsymbol{\delta}^{i+1}(\boldsymbol{x}) = \boldsymbol{\lambda}^i(\boldsymbol{x}) - \boldsymbol{L}^0 \breve{\boldsymbol{\varepsilon}}^i(\boldsymbol{x})$. Next, $\hat{\boldsymbol{\delta}}^{i+1}(\boldsymbol{\xi}) = ftt\{\boldsymbol{\delta}^{i+1}(\boldsymbol{x})\}$ is computed, where *ftt* is the discrete Fourier transform operator (numerically implemented by means of the FFT algorithm). It follows that the new guess for the *kinematically admissible* strain-rate deviation field is obtained as

$$\hat{\breve{\boldsymbol{\epsilon}}}^{i+1}(\boldsymbol{\xi}) = -\hat{\boldsymbol{\varGamma}}^0(\boldsymbol{\xi})\hat{\boldsymbol{\delta}}^i(\boldsymbol{\xi}), \quad \forall \boldsymbol{\xi} \neq \boldsymbol{0} \quad \text{and} \quad \hat{\breve{\boldsymbol{\epsilon}}}^{i+1}(\boldsymbol{0}) = \boldsymbol{0}.$$

The corresponding field in real space is thus obtained by application of the inverse FFT, i.e.

$$\breve{\boldsymbol{\epsilon}}^{i+1}(\boldsymbol{x}) = ftt^{-1}\{\hat{\breve{\boldsymbol{\epsilon}}}^{i+1}(\boldsymbol{\xi})\},$$

and the new guess for the deviatoric stress field is calculated from (Michel *et al.* 2000)

$$\boldsymbol{\sigma}^{i+1}(\boldsymbol{x}) + \boldsymbol{L}^0 \boldsymbol{\varepsilon}^{i+1}(\boldsymbol{x}) = \boldsymbol{\lambda}^i(\boldsymbol{x}) + \boldsymbol{L}^0(\boldsymbol{E} + \breve{\boldsymbol{\epsilon}}^{i+1}(\boldsymbol{x})), \tag{2.25}$$

where

$$\boldsymbol{\varepsilon}^{i+1}(\boldsymbol{x}) = \left.\frac{\partial u(\boldsymbol{x}, \boldsymbol{\sigma})}{\partial \boldsymbol{\sigma}}\right|_{\sigma^{i+1}(\boldsymbol{x})}. \tag{2.26}$$

Hence, using the local constitutive relations (2.1)–(2.3) explicitly, (2.25) can be written as

$$\boldsymbol{\sigma}^{i+1}(\boldsymbol{x}) + \boldsymbol{L}^0 \sum_{k=1}^K \gamma_0 \left(\frac{\boldsymbol{\sigma}^{i+1}(\boldsymbol{x}) \cdot \boldsymbol{\mu}_{(k)}^{(r)}}{(\tau_0)_{(k)}}\right)^n \boldsymbol{\mu}_{(k)}^{(r)} = \boldsymbol{\lambda}^i(\boldsymbol{x}) + \boldsymbol{L}^0(\boldsymbol{E} + \breve{\boldsymbol{\epsilon}}^{i+1}(\boldsymbol{x})). \tag{2.27}$$

Expression (2.27) is a system of nonlinear equations whose solution gives $\boldsymbol{\sigma}^{i+1}(\boldsymbol{x})$ $\forall \boldsymbol{x} \in \{\boldsymbol{x}_\mathrm{d}\}$. To complete the iteration, the new guess of the Lagrange multiplier field (Michel *et al.* 2000) is obtained from

$$\boldsymbol{\lambda}^{i+1}(\boldsymbol{x}) = \boldsymbol{\lambda}^i(\boldsymbol{x}) + \boldsymbol{L}^0(\boldsymbol{\epsilon}^{i+1}(\boldsymbol{x}) - \boldsymbol{\varepsilon}^{i+1}(\boldsymbol{x})). \tag{2.28}$$

Expressions (2.27) and (2.28) guarantee the convergence of (a) $\boldsymbol{\varepsilon}(\boldsymbol{x})$ (i.e. the strain-rate field related with the stress through the constitutive equation) towards $\boldsymbol{\epsilon}(\boldsymbol{x})$ (i.e. the kinematically admissible strain-rate field) to fulfil compatibility, (b) the Lagrange multiplier field $\boldsymbol{\lambda}(\boldsymbol{x})$ towards the stress field $\boldsymbol{\sigma}(\boldsymbol{x})$ to fulfil equilibrium.

(iii) *Convergence test*

Based on the above discussion, the obvious choice of a convergence criterion after the jth iteration is given by

$$\mathrm{err}(\boldsymbol{\varepsilon}) = \frac{\langle \|\boldsymbol{\varepsilon}^j(\boldsymbol{x}) - \boldsymbol{\epsilon}^j(\boldsymbol{x})\|_2 \rangle}{E_\mathrm{e}} < \delta, \qquad \mathrm{err}(\boldsymbol{\sigma}) = \frac{\langle \|\boldsymbol{\sigma}^j(\boldsymbol{x}) - \boldsymbol{\lambda}^j(\boldsymbol{x})\|_2 \rangle}{\Sigma_\mathrm{e}} < \delta, \tag{2.29}$$

where $\|\cdot\|_2$ denotes the quadratic norm, E_e and Σ_e are the macroscopic equivalent strain rate and stress, and δ is a small positive threshold quantity.

3. Power-law, 2D polycrystals under anti-plane strain

(a) Formulation

In this section, the focus is on a special class of model polycrystals consisting of columnar orthorhombic grains, such that the grains are cylindrical in shape and their symmetry axes are all aligned with the x_3-axis. When such polycrystals are loaded in anti-plane strain, only two slip systems are activated. They are those defined by the Schmid tensors:

$$\boldsymbol{\mu}_{(1)} = \tfrac{1}{2}(\boldsymbol{e}_1 \otimes \boldsymbol{e}_3 + \boldsymbol{e}_3 \otimes \boldsymbol{e}_1), \qquad \boldsymbol{\mu}_{(2)} = \tfrac{1}{2}(\boldsymbol{e}_2 \otimes \boldsymbol{e}_3 + \boldsymbol{e}_3 \otimes \boldsymbol{e}_2). \qquad (3.1)$$

Therefore, a 2D boundary-value problem is defined, where the non-zero components of the stress and strain rate tensors, σ_{13}, σ_{23}, ε_{13} and ε_{23} are functions of x_1 and x_2 only.

Although more general constitutive behaviours could be considered for the constituent grains, for simplicity the stress potentials will be assumed here to be of the power-law type (2.3), with the same exponent n for both systems. It follows, by further assuming that the statistical distribution of the grains in the transverse plane is isotropic both in space and orientation (i.e. isotropic crystallographic texture and equi-axed grains in the plane), that the polycrystal will exhibit isotropic properties in the plane. Therefore, under anti-plane strain conditions, the effective behaviour of the polycrystal is fully determined by the *effective flow stress*, $\tilde{\sigma}_0$, appearing in the expressions for the effective potentials,

$$\tilde{U}(\boldsymbol{\Sigma}) = \frac{\gamma_0 \tilde{\sigma}_0}{n+1}\left(\frac{\Sigma_e}{\tilde{\sigma}_0}\right)^{n+1}, \qquad \tilde{W}(\boldsymbol{E}) = \frac{\gamma_0 \tilde{\sigma}_0}{m+1}\left(\frac{E_e}{\gamma_0}\right)^{1+m}, \qquad (3.2)$$

where

$$\Sigma_e = \sqrt{3}[\Sigma_{13}^2 + \Sigma_{23}^2]^{1/2}, \qquad E_e = \tfrac{2}{\sqrt{3}}[E_{13}^2 + E_{23}^2]^{1/2}.$$

In what follows, because of the anti-plane strain conditions and for consistency with earlier work, we will make use of the effective *shear* flow stress or *effective viscosity*: $\tilde{\tau}_0 = \tilde{\sigma}_0/3^{(n+1)/(2n)}$, rather than referring to $\tilde{\sigma}_0$.

Given that for this class of polycrystals the grain orientation (r) can be uniquely identified with an angle $\theta^{(r)}$, defined such that $\theta^{(r)} = 0$ corresponds to the orientation of grains with the normal to system (1) aligned with the sample direction x_1, the dependence on $\theta^{(r)}$ for the phase averages and fluctuations of the relevant components of the stress and strain-rate fields will be investigated below. In this connection, it is useful to introduce some additional notation for later use. Thus, recalling the definitions (2.18) and (2.23)$_1$ for the phase averages of the resolved shear stresses and slip rates, corresponding equivalent measures associated with the phase averages of the stress $\bar{\boldsymbol{\sigma}}^{(r)}$ and strain rate $\bar{\boldsymbol{\varepsilon}}^{(r)}$ are defined by

$$\bar{\sigma}_e^{(r)} = \sqrt{3}[(\bar{\sigma}_{13}^{(r)})^2 + (\bar{\sigma}_{23}^{(r)})^2]^{1/2}, \qquad \bar{\varepsilon}_e^{(r)} = \tfrac{2}{\sqrt{3}}[(\bar{\varepsilon}_{13}^{(r)})^2 + (\bar{\varepsilon}_{23}^{(r)})^2]^{1/2}, \qquad (3.3)$$

where $\bar{\sigma}_{13}^{(r)} = \langle \sigma_{13} \rangle^{(r)}$, $\bar{\varepsilon}_{13}^{(r)} = \langle \varepsilon_{13} \rangle^{(r)}$, and similarly for the other two components of the stress and strain-rate tensors. It will also be useful to introduce the notation $\bar{\bar{\tau}}_{(k)}^{(r)}$ and $\bar{\bar{\gamma}}_{(k)}^{(r)}$ for the second moments of the resolved shear stresses and strains, as given by

$$\bar{\bar{\tau}}_{(k)}^{(r)} = \sqrt{\langle (\tau_{(k)}^{(r)})^2 \rangle^{(r)}} = \sqrt{\boldsymbol{\mu}_{(k)}^{(r)} \cdot \langle \boldsymbol{\sigma} \otimes \boldsymbol{\sigma} \rangle^{(r)} \boldsymbol{\mu}_{(k)}^{(r)}}, \qquad (3.4)$$

with a completely analogous expression for $\bar{\bar{\gamma}}^{(r)}_{(k)}$. Similarly,

$$\bar{\bar{\sigma}}^{(r)}_{13} = \sqrt{\langle \sigma^2_{13} \rangle^{(r)}}, \qquad \bar{\bar{\sigma}}^{(r)}_{23} = \sqrt{\langle \sigma^2_{23} \rangle^{(r)}},$$

so that the second moment of the equivalent stress over grains with orientation $\theta^{(r)}$ is defined via

$$\bar{\bar{\sigma}}^{(r)}_{\mathrm{e}} = \sqrt{\langle \sigma^2_{\mathrm{e}} \rangle^{(r)}} = \sqrt{3}[(\bar{\bar{\sigma}}^{(r)}_{13})^2 + (\bar{\bar{\sigma}}^{(r)}_{23})^2]^{1/2}, \tag{3.5}$$

with analogous expressions for $\bar{\bar{\varepsilon}}^{(r)}_{13}$, $\bar{\bar{\varepsilon}}^{(r)}_{23}$, and $\bar{\bar{\varepsilon}}^{(r)}_{\mathrm{e}}$. In addition, the standard deviations of the stress and strain-rate fields over grains with orientation $\theta^{(r)}$ are given by expressions of the type

$$\mathrm{SD}^{(r)}(\tau^{(r)}_{(k)}) = \sqrt{(\bar{\bar{\tau}}^{(r)}_{(k)})^2 - (\bar{\tau}^{(r)}_{(k)})^2} = |\hat{\tau}^{(r)}_{(k)} - \bar{\tau}^{(r)}_{(k)}|. \tag{3.6}$$

Finally, it is useful to also define field statistics over the whole polycrystal, such as the second moments of the equivalent stress $\bar{\bar{\sigma}}_{\mathrm{e}} = \sqrt{\langle \sigma^2_{\mathrm{e}} \rangle}$, and the standard deviation of the von Mises stress,

$$\mathrm{SD}(\sigma_{\mathrm{e}}) = \sqrt{\bar{\bar{\sigma}}^2_{\mathrm{e}} - \Sigma^2_{\mathrm{e}}}, \tag{3.7}$$

with completely analogous expressions for the second moment and standard deviation of the equivalent strain rate, denoted $\bar{\bar{\varepsilon}}_{\mathrm{e}}$ and $\mathrm{SD}(\varepsilon_{\mathrm{e}})$, respectively.

(b) Bounds and estimates

This special class of 2D polycrystals has received considerable attention in the literature in recent years, in spite of its somewhat limited practical value. This is due to the fact that this problem is known (Dykhne 1970) to have an exact solution, $\tilde{\tau}_0 = \sqrt{(\tau_0)_{(1)}(\tau_0)_{(2)}}$, when the behaviour of the single crystals is linear ($n = m = 1$). For more general power-law polycrystals with $n, m \neq 1$, the exact result is not known, but upper and lower bounds are available. These include the Taylor and Kohn–Little (Kohn & Little 1998) upper bounds, as well as the Reuss lower bounds. Explicit expressions of these bounds for $\tilde{\tau}_0$ have been given, for example, in Ponte Castañeda & Nebozhyn (1997). It is noted that the Kohn–Little upper bound is usually (but not always) sharper than the Taylor upper bound, especially for large values of the anisotropy parameter $M = (\tau_0)_{(2)}/(\tau_0)_{(1)}$, when it scales as $M^{1/2}$, as opposed to the Taylor bound, which scales as M^1. The Reuss lower bound, on the other hand, scales as M^0 for large M. Upper bounds that improve on both the Kohn–Little and Taylor bounds have been given by Nesi *et al.* (2000) and Goldstein (2001) for the special case of *ideally plastic* ($m = 0$) polycrystals. The former are the best known bounds for small values of the anisotropy parameter M, and the latter for larger values of M.

Unfortunately, the range of possible behaviours allowed by these bounds is still quite large, especially at large values of M ($M^{1/2}$ versus M^0). In addition, only the classical Taylor and Reuss bounds are available for more realistic classes of 3D polycrystals, such as FCC and HCP polycrystals. For this reason, considerable use has been made in the literature of the self-consistent approximation, which was originally developed (Hershey 1954; Kröner 1958; Willis 1977) for 3D polycrystals with linear constitutive behaviour. As already mentioned, there are several generalizations of the self-consistent approximation that have been proposed over the years for polycrystals with nonlinear constitutive behaviour (plasticity and viscoplasticity). Now, it is

known (Ponte Castañeda & Nebozhyn 1997) that the standard SC approximation predicts the exact result $\tilde{\tau}_0 = \sqrt{(\tau_0)_{(1)}(\tau_0)_{(2)}}$ for the above class of 2D polycrystals in the limit of linear constitutive behaviour ($n = m = 1$). This strongly suggests comparing the various nonlinear generalizations of the SC approximation with the above bounds and with the predictions of the FFT simulations for this specific class of problems. This will be carried out in some detail in §4. In addition, noting that the 'second-order' method discussed in §2 b has the capability of also providing estimates for the per-phase averages and fluctuations of the stress and strain-rate fields in the polycrystal, comparisons will also be carried out in §4 with the corresponding FFT results. In this connection, it is noted here for later reference that the standard SC approximation may be used to generate analytical expressions for the phase averages and fluctuations of the stress and strain-rate fields for the case of a linear ($n = 1$) 2D polycrystal. For example, the per-phase averages and SD of the resolved shear stresses are given by

$$\bar{\tau}_{(1)}^{(r)} = \frac{2\cos\theta\,\Sigma_{\mathrm{e}}}{\sqrt{3}(1+\sqrt{M})}, \qquad \bar{\tau}_{(2)}^{(r)} = -\frac{2\sin\theta\,\Sigma_{\mathrm{e}}}{\sqrt{3}(1+\sqrt{M})},$$

$$\mathrm{SD}^{(r)}(\tau_{(2)}^{(r)}) = M^{1/2}\,\mathrm{SD}^{(r)}(\tau_{(1)}^{(r)}) = \frac{(\sqrt{M}-1)M^{1/4}\Sigma_{\mathrm{e}}}{\sqrt{6}(1+\sqrt{M})},$$

while the second moment of the equivalent stress over the whole polycrystal is given by

$$\bar{\bar{\sigma}}_{\mathrm{e}} = \sqrt{\frac{1+M}{2M^{1/2}}}\,\Sigma_{\mathrm{e}},$$

which scales as $M^{1/4}$ for large values of M.

(c) Ensemble averages over FFT solutions

The expected value of any experiment performed on stochastic systems is the mean of the outcomes of many experiments which are alike in a macro sense but differ in micro details (Kröner 1986). This suggests that one way of getting effective properties is by performing *ensemble averages*, i.e. averages over the outcomes of the same experiment performed on many specimens which are prepared alike but differ at the micro-level, due to its inherent stochastic character. Using the *ergodic hypothesis* for systems that are stochastic in space, an alternative approach would be to make use of *volume averages* over a single volume element, which should be large enough to be representative of the microstructure considered. With this in mind, a periodic 2D polycrystal is first considered, which is generated by periodic repetition of a square unit cell consisting of square grains, such that the unit cell has $32 \times 32 = 1024$ grains. If this unit cell is discretized using a 256×256 Fourier grid, this results in $8 \times 8 = 64$ Fourier points per grain. However, for such a specimen with equi-axed grains, even if its crystallographic orientations are chosen at random, and the constitutive behaviour linear ($n = 1$ in (2.3)), it has been verified that the FFT solution of the anti-plane deformation of such a linear 2D polycrystal leads, in general, to a slightly non-isotropic response (Lebensohn *et al.* 2004). Thus, for an applied strain-rate tensor with only one non-zero independent component (say, E_{13}), the resulting stress tensor would be expected to have a small, but non-vanishing

component Σ_{23} (in addition to a non-zero Σ_{13}). Consequently, the effective viscosity $\tilde{\tau}_0$ deviates from the theoretical value $\sqrt{(\tau_0)_{(1)}(\tau_0)_{(2)}}$. This result would suggest that a unit cell of such dimensions is not actually representative of the class of isotropic polycrystals with random microstructure. For this to be true, it would be necessary to have a very large volume element, containing a large number of different grains with the same orientation but different environments. Evidently, the size of a unit cell (and the Fourier grid needed for its discretization) that would fulfil the above condition (while keeping a large number of Fourier points inside each grain to capture intragranular heterogeneities) would require numerical capabilities far beyond our available resources. In fact, our periodic unit cell is representative of a periodic polycrystal generated by periodic repetition of that unit cell in both directions of the space. The response of this periodic polycrystal is equivalent to that of one specimen in an ensemble. Therefore, the averages over a sufficiently large number of periodic unit cell configurations should give the effective properties of a polycrystal with random microstructure. With this in mind, and in order to compare macroscopic and per-phase quantities obtained from FFT simulations with analogous quantities obtained from SC formulations for aggregates with random microstructure, 100 different periodic unit cells have been constructed using the following procedure.

(i) The square grains in the 2D array described above were numbered from 1 to 1024.

(ii) 100 random sequences of 1024 angles between -180 and $180°$ were generated.

(iii) Each sequence was scanned to find the angles having the minimum distances from certain special orientations, $\{\theta^{(r)}\} = \{0, 10, 20, 30, 40, 50, 60, 70, 80, 90°\}$, which were selected for ensemble averaging of the per-phase statistical quantities. The angles having those minimum distances were redefined as $0, 10, \ldots,$ $90°$, respectively. In this way, these 10 orientations were present in every unit cell, surrounded by different environments, which in turn were randomly chosen. It is worth noting that in all cases, the minimum distances to the marked orientations were less than $0.5°$, so that the perturbation to the randomness of the set of angles was negligible.

(iv) To construct the αth configuration, the first angle of the αth random sequence was assigned to grain 1, the second angle to grain 2, and so on.

Using the superscript $[\alpha]$ to denote a single configuration, i.e. $\boldsymbol{E}^{[\alpha]} = \langle \boldsymbol{\varepsilon}^{[\alpha]} \rangle$ and $\boldsymbol{\Sigma}^{[\alpha]} = \langle \boldsymbol{\sigma}^{[\alpha]} \rangle$, the ensemble averages of macroscopic magnitudes are given by

$$\boldsymbol{E} = \frac{1}{N_\alpha} \sum_{\alpha=1}^{N_\alpha} \boldsymbol{E}^{[\alpha]}, \qquad \boldsymbol{\Sigma} = \frac{1}{N_\alpha} \sum_{\alpha=1}^{N_\alpha} \boldsymbol{\Sigma}^{[\alpha]}, \tag{3.8}$$

where N_α is the number of unit cell configurations. Note that the effective viscosity can be calculated from ensemble average magnitudes as $\tilde{\tau}_0 = \Sigma_{13}/(2\dot{E}_{13})^{1/n}$. The ensemble averages of per-phase and overall first and second moments are also made consistent with prior definitions. For example, in the case of the 'anti-plane' stress component, they are

$$\bar{\sigma}_{13}^{(r)} = \frac{1}{N_\alpha} \sum_{\alpha=1}^{N_\alpha} \langle \sigma_{13}^{[\alpha]} \rangle^{(r)}, \qquad \bar{\bar{\sigma}}_{13}^{(r)} = \left[\frac{1}{N_\alpha} \sum_{\alpha=1}^{N_\alpha} \langle (\sigma_{13}^{[\alpha]})^2 \rangle^{(r)} \right]^{1/2} \tag{3.9}$$
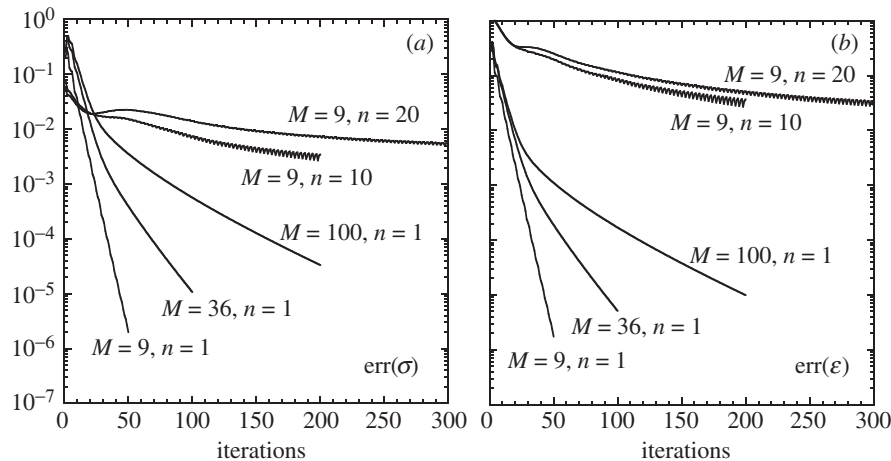
Figure 1. Evolution of the relative errors as functions of the number of iterations, for different values of M and n: (a) stress and (b) strain-rate fields.

Table 1. *Adopted number of iterations and average relative errors, for different values of M and n*

M	n	iterations	err($\boldsymbol{\sigma}$)	err($\boldsymbol{\varepsilon}$)
9	1	50	0.183×10^{-5}	0.165×10^{-5}
36	1	100	0.107×10^{-4}	0.525×10^{-5}
100	1	200	0.334×10^{-4}	0.101×10^{-4}
9	10	250	0.347×10^{-2}	0.159×10^{-1}
9	20	300	0.506×10^{-2}	0.188×10^{-1}

Finally, in order to assess the accuracy of the foregoing ensemble average approach, the convergence of the FFT method was studied for a single RVE configuration and for different contrasts and rate sensitivities, as well as the convergence (stabilization) of the ensemble averages of the phase statistical moments, as the number of configurations in the ensemble is increased. Thus, figure 1 shows the evolution of err($\boldsymbol{\sigma}$) and err($\boldsymbol{\varepsilon}$) (see equations (2.29)) for a single configuration, as the number of iterations increases, for $n = 1$ and different contrasts, and for $M = 9$ and different rate sensitivities. It is seen that, although the FFT calculations converge (i.e. the error indicators decrease) for every set of parameters considered here, reaching errors smaller than a given threshold requires to increase the number of iterations as the contrast or the nonlinearity of the material increase.

Due to the very distinct behaviours, shown above for different contrasts and non-linearities, of the error indicators in the foregoing ensemble average calculations, it was decided to use a *fixed* (manageable) number of iterations instead of considering a unique threshold error δ, for each pair of M and n. Table 1 shows the number of iterations adopted and the resulting relative errors, averaged over the different RVE configurations, for $n = 1$ and different contrasts, and for $M = 9$ and different rate sensitivities. While in the linear cases an affordable number of iterations allows
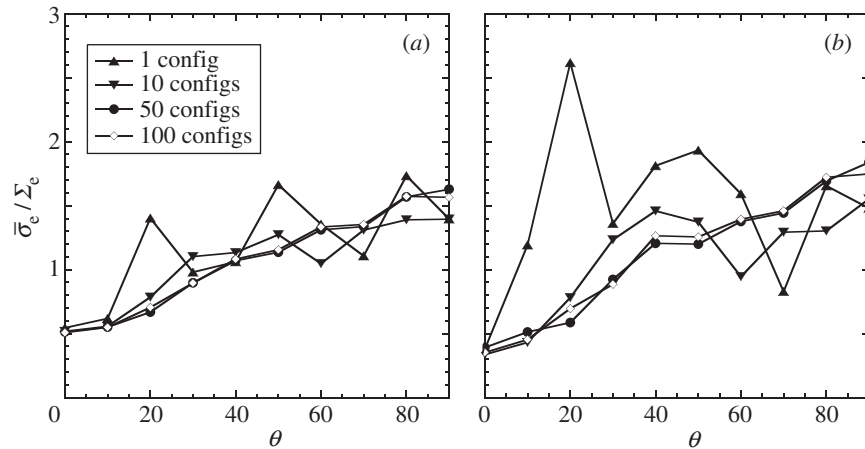
Figure 2. Ensemble averages of the per-phase first moments of the von Mises stress as functions of the phase orientation angle θ, for an increasing number of configurations, for $M = 9$ and (a) $n = 1$, (b) $n = 10$.

reaching very low convergence errors, in the nonlinear cases the relative errors remain in the order of 1%, the strain-rate errors being higher than the stress errors.

Concerning the number of configurations needed to obtain representative ensemble averages, figure 2 shows the ensemble averages of per-phase first moments of the equivalent stress (normalized with the ensemble average equivalent stress) as a function of the phase orientation angle, for $M = 9$ and different rate sensitivities, as the number of configurations increases. It is worth mentioning that, if the stress in the phase were dictated only by its relative orientation, $\bar{\sigma}_e / \Sigma_e$ versus angle should be a monotonically increasing curve (note that, for anti-plane deformation, the soft slip system has the highest possible Schmid factor in the phase at 0°, and that this factor decreases as the phase angle increases, reaching a null value at 90°). However, for a single configuration, the curves show a marked non-monotonic behaviour, suggesting that the phase response is affected as much by its neighbours as by its orientation. Moreover, the range of variation and the jumps of the curves are higher in the nonlinear case. For 10 configurations, the curves become smoother but still display some non-monotonic behaviour. The curves for an ensemble of 50 configurations are already monotonic (although presenting several inflexion points), meaning that the influences of the different phase environments have been averaged out, resulting in ensemble averages of the per-phase moments that are mainly dictated by the phase orientation. Finally, the phase moments obtained for 100 configurations remain practically the same as those for 50 configurations, indicating a desirable stabilization of the calculated averages.

4. Results

In this section, the 'second-order' SC estimates for the effective behaviour and field heterogeneity of the model 2D power-law polycrystals are compared with the corresponding results arising from the FFT simulations, as well as with the Taylor, Kohn–Little and Reuss bounds. In addition, some comparisons are included with other nonlinear generalizations of the SC method for nonlinear systems, including

the 'incremental' method (Hill 1965; Hutchinson 1976), the 'tangent' method (Molinari *et al.* 1987; Lebensohn & Tomé 1993), and the 'variational' method (deBotton & Ponte Castañeda 1995; Ponte Castañeda & Nebozhyn 1997).

In figure 3, the 'second-order' SC estimates for the effective viscosity $\tilde{\tau}_0$ are shown and compared with the FFT simulation results. Note that the 'error' bars for the FFT results correspond to the maximum and minimum values of $\tilde{\tau}_0$ over all configurations (100 and 50 for figure 3*a* and figure 3*b*, respectively). Figure 3*a* shows results for $\tilde{\tau}_0$ plotted as functions of the strain-rate sensitivity $m = 1/n$, for a fixed value of the grain anisotropy ($M = 9$). Note that the Taylor, Reuss and Kohn–Little bounds, as well as the 'variational' SC estimates, are included in this figure. In addition, both the 'energy' (continuous line) and the 'constitutive relation' (dashed line) versions of the 'second-order' estimates are shown (cf. (2.17) and (2.22)). It can be seen from this figure that the 'variational' as well as both versions of 'second-order' SC estimates are consistent with the upper and lower bounds, and agree exactly with the Kohn–Little bound for $m = 1/n = 1$. But these two types ('variational' versus 'second order') of SC estimates become progressively more different as m tends to zero, where the 'variational' estimate is nearly twice the 'second-order' estimates. The key observation, however, is that the 'second-order' SC estimates (both versions) are fairly consistent with the FFT results, while the 'variational' SC estimates largely overestimate the numerical results (recall that they are upper bounds for all other SC estimates (Ponte Castañeda & Nebozhyn 1997)). Because the differences between the two versions of the 'second-order' SC estimates are relatively small in general (see also Liu & Ponte Castañeda 2003), and for simplicity, only the 'energy' version will be shown in the results below. Figure 3*b* shows the results for the various bounds and SC estimates for $\tilde{\tau}_0$ as functions of the grain anisotropy M, for a fixed value of the nonlinearity ($n = 1/m = 10$). Among the SC estimates shown in this figure for comparison purposes are the 'incremental' and 'tangent' SC estimates. The main observation is that the 'second-order' estimate is the *only one* that is consistent with the FFT results. Interestingly, it appears to lie roughly midway between the 'variational' and 'tangent' SC estimates. It is emphasized that at this fairly typical value of the strain-rate sensitivity ($m = 0.1$) the bounds and other SC estimates can lead to large errors for large values of the grain anisotropy parameter. For example, at a value of $M = 9$, the Taylor bound and 'incremental' estimate would lead to predictions that are more than twice the FFT predictions, while the 'variational' and 'tangent' estimates would lead to predictions that are *ca.* 40% larger and 35% lower, respectively. (Note, however, that the 'tangent' estimates are accurate for small enough values of M.)

Figure 4*a*,*b* provides results for the effective viscosity for a larger range of values of the anisotropy parameter M, plotted in logarithmic scales, for $n = 1$ and 10, respectively. As shown in figure 4*a*, the SC estimates which are exact in the linear case ($n = 1$) serve as a check on the FFT simulations, and it can be seen that they are quite accurate up to values of $M = 10^4$, when the simulations begin to deviate significantly from the exact results, which correspond to a straight line with slope $\frac{1}{2}$. (Note that $\tilde{\tau}_0/(\tau_0)_{(1)}|_{M=10^5} = 311.9$ and $\tilde{\tau}_0/(\tau_0)_{(1)}|_{M=10^6} = 849.9$, i.e. 1.4% and 15.0% underestimation of the theoretical values $10^{5/2} = 316.2$ and $10^3 = 1000$, respectively.) It is believed that these deviations are due to the large fluctuations in the local fields within the polycrystal, which may not be captured very accurately with the grid refinement adopted (256×256), and/or to the impossibility of reaching convergence
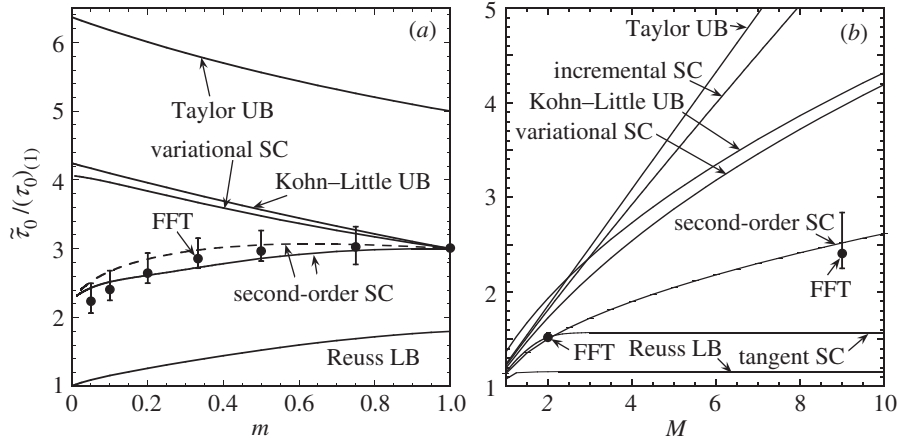
Figure 3. Comparison of the 'second-order' SC estimates with the FFT simulation results, and the Taylor, Kohn–Little and Reuss bounds for the effective viscosity $\tilde{\tau}_0$ as functions of (a) the strain-rate sensitivity m for $M = (\tau_0)_{(2)}/(\tau_0)_{(1)} = 9$; (b) the grain anisotropy M for $n = 1/m = 10$. Also shown in parts (a) and (b) are the 'variational' SC estimates, and in part (b) the 'incremental' and 'tangent' SC estimates.
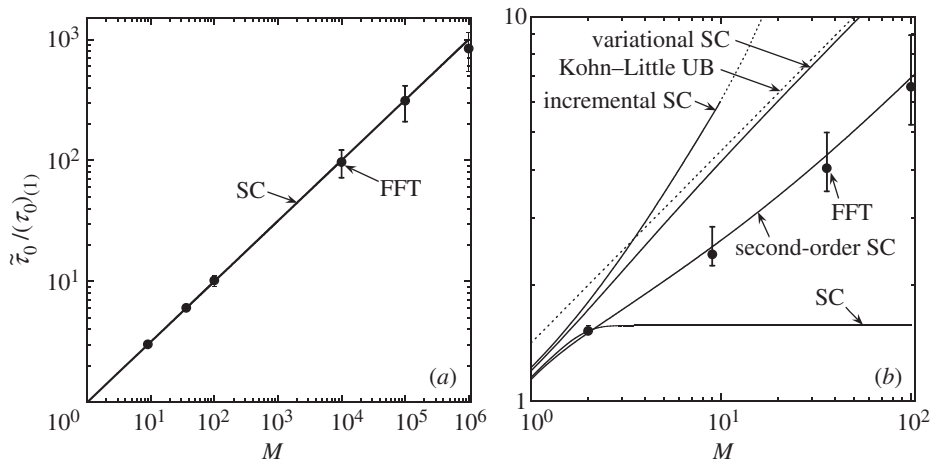

Figure 4. Log–log comparison of the various ('incremental', 'variational', 'second-order' and 'tangent') SC estimates with the FFT estimates and the Kohn–Little upper bound for the effective viscosity $\tilde{\tau}_0$ as a function of the contrast $M = (\tau_0)_{(2)}/(\tau_0)_{(1)}$ for (a) $n = 1/m = 1$, (b) $n = 10$.

errors smaller than a few per cent, for high contrasts and low rate sensitivities, as shown in table 1. It is emphasized that the number of Fourier points and the number of iterations used for these FFT calculations were the maximum allowed by the size and the speed of our available computational resources. On the other hand, figure 4b clearly shows that the various SC estimates give widely diverging trends for large values of M, in this strongly nonlinear case ($n = 10$). Thus, the 'incremental' and 'tangent' SC estimates predict large-M trends that are consistent with linear growth (M^1) and no growth (M^0), respectively. In contrast, both the 'variational'
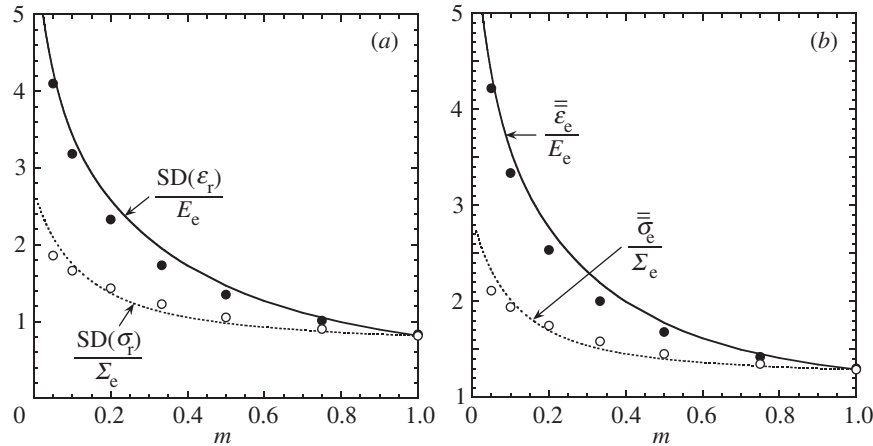
Figure 5. Comparison of the 'second-order' SC (lines) and FFT (circles) estimates for the field fluctuations and second moments of the stress and strain rates over the polycrystal, as functions of the strain rate sensitivity m, for grain anisotropy $M = 9$. (a) Standard deviations of the field fluctuations of the von Mises stress $\mathrm{SD}(\sigma_e)$ and the equivalent plastic strain rate $\mathrm{SD}(\varepsilon_e)$. (b) Second moments of the von Mises stress $\bar{\bar{\sigma}}_e$ and the equivalent plastic strain rate $\bar{\bar{\varepsilon}}_e$. The results are normalized by the applied stress Σ_e and the applied strain rate E_e, respectively.

and 'second-order' estimates give trends that are consistent with square-root growth. That is, they both grow like $aM^{1/2}$, for sufficiently large values of M. However, the 'second-order' SC estimates give better overall agreement with the FFT results than the other models, capturing not only the correct exponent $(\tfrac{1}{2})$, but also the correct coefficient a. It is emphasized that the numerical results for the 'variational' and 'second-order' estimates suggest that the power $(\tfrac{1}{2})$ is independent of n, but that the coefficient a does depend on n. In addition, it should be mentioned that, while exact estimates are not available for comparison in the nonlinear case, the above comparisons for the linear case suggest that the nonlinear FFT results could be inaccurate at the higher values of the contrast M.

Figure 5a, b shows plots of the 'second-order' SC (continuous and dashed lines) and FFT (dark and clear circles) estimates for the m-dependence of the fluctuations and second moments of the stress and strain rate, for a fixed value of the grain anisotropy ($M = 9$). More specifically, figure 5a shows plots of the standard deviations of the von Mises stress $\mathrm{SD}(\sigma_e)$ (see relation (3.7)) and the equivalent plastic strain rate $\mathrm{SD}(\varepsilon_e)$, normalized by the average von Mises stress Σ_e and equivalent plastic strain rate E_e, respectively. The main observation in the context of this figure is that both the stress and the strain-rate fluctuations grow with decreasing values of m (increasing nonlinearity n). Furthermore, it can be seen that the 'second-order' SC estimates give excellent agreement with the FFT results, even at the lower values of m. In addition, the strain-rate fluctuations are seen to grow at a progressively faster rate than the stress fluctuations as the nonlinearity increases. This behaviour is consistent with the localization of the deformation field (into shear bands) in the grains of the polycrystals in the limit as m tends to zero (Suquet 2001; Bhattacharya & Suquet 2004). Figure 5b shows plots of the corresponding second moments $\bar{\bar{\sigma}}_e$ and $\bar{\bar{\varepsilon}}_e$, normalized in similar fashion. These plots are essentially the same as those shown in figure 5a, apart from a shift which is noticeable only for small values of M and
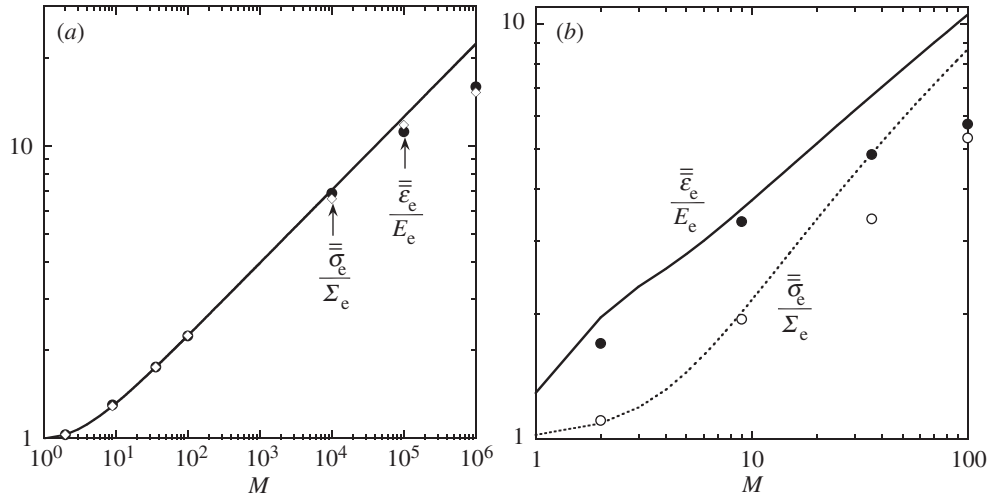
Figure 6. Comparison of the 'second-order' SC (lines) and FFT (circles) estimates for the second moments of the equivalent stress $\bar{\bar{\sigma}}_e$ and the equivalent plastic strain rate $\bar{\bar{\varepsilon}}_e$ over the polycrystal, as functions of the grain anisotropy M. (a) $n = 1$, (b) $n = 10$. The results for $\bar{\bar{\sigma}}_e$ and $\bar{\bar{\varepsilon}}_e$ are normalized by Σ_e and E_e, respectively.

n. For this reason, in the rest of this section, only second-moment quantities will be shown, the corresponding fluctuation quantities being easily derived from these.

Figure $6a, b$ shows plots of the M-dependence of the 'second-order' SC (lines) and FFT (circles) estimates for the second moments of the von Mises stress $\bar{\bar{\sigma}}_e$ and strain rate $\bar{\bar{\varepsilon}}_e$, respectively, for fixed values of n ($n = 1$ and 10). It is seen that the second moments of the stress and strain rate (as well as the corresponding fluctuations) grow with M. It is emphasized that the results given in figure $6a$ for the linear case have been calculated explicitly from the SC expressions (refer to the expressions at the end of § 3 b), and are conjectured—as the corresponding results for the effective shear flow stress—to be exact (or at least very accurate). They can therefore be used to calibrate the FFT simulations. Thus, it can be seen from figure $6a$ that, while the FFT results are very accurate for values of M up to 100, the FFT simulations start to deviate from the exact results for values of M greater than 10^4. This loss of accuracy for large values of M is consistent with earlier observations concerning effective magnitudes calculated by means of the FFT approach. Figure $6b$ gives the corresponding results for a highly nonlinear case ($n = 10$). It can be deduced from this figure that the stress and strain-rate fluctuations become different in the nonlinear case, with larger fluctuations in the strain rate than in the stress, as would be expected for a low-hardening material. However, although the 'second-order' SC estimates and the FFT results exhibit similar trends, significant differences in their predictions are observed for values of M greater than about 10. While this value of M (for the nonlinear problem) may seem relatively small, it is in fact effectively quite large. This is because a nonlinear system with grain anisotropy M and nonlinearity n would be expected to behave roughly like a linear system with grain anisotropy M^n (Liu & Ponte Castañeda 2003). Because significant errors have already been identified in the FFT simulations for the linear polycrystal at sufficiently high values of M, corresponding errors would be expected in the present nonlinear FFT simulations,

at much smaller values of M. Of course, this does not necessarily imply that the 'second-order' SC estimates are accurate. As with any approximation, errors would be expected, especially at these high nonlinearities and contrasts. However, it seems plausible that at least *some* of the differences observed at high M in the FFT-versus-'second-order' comparisons of figure 6*b* could be due to inaccuracies associated with the FFT simulations.

Next the 'second-order' SC predictions are compared with the corresponding FFT results for the *r*-phase averages and second moments of the resolved shear stresses and slip rates

$$(\bar{\tau}_{(1)}^{(r)}, \bar{\tau}_{(2)}^{(r)}, \bar{\bar{\tau}}_{(1)}^{(r)}, \bar{\bar{\tau}}_{(2)}^{(r)}, \bar{\gamma}_{(1)}^{(r)}, \bar{\gamma}_{(2)}^{(r)}, \bar{\bar{\gamma}}_{(1)}^{(r)}, \bar{\bar{\gamma}}_{(2)}^{(r)}),$$

plotting them as functions of the grain orientation $\theta^{(r)}$. It is recalled that $\theta^{(r)}$ is the angle from the normal vector of the soft slip system (1) to the direction of applied loading.

Figure 7 provides comparisons of the 'second-order' SC estimates (lines) and FFT results (symbols) for the average resolved shear stresses $\bar{\tau}_{(1)}^{(r)}$ and $\bar{\tau}_{(2)}^{(r)}$, as well as the corresponding second moments $\bar{\bar{\tau}}_{(1)}^{(r)}$ and $\bar{\bar{\tau}}_{(2)}^{(r)}$ (over grains with fixed orientation $\theta^{(r)}$), plotted as functions of $\theta^{(r)}$. Figure 7*a*–*d* is for a fixed value of the grain anisotropy ($M = 9$) and for several values of the nonlinearity ($n = 1, 3, 5, 10$, respectively). The overall agreement is seen to be quite satisfactory, especially for small nonlinearity ($n = 1, 3$), and it is generally better for the hard systems. At the larger values of the nonlinearity n, the 'second-order' estimates for the average shear stresses on the soft systems $\bar{\tau}_{(1)}^{(r)}$ seem to be systematically larger than the corresponding results for FFT, and the differences become more pronounced for values of $\theta^{(r)}$ near, but not equal to, 90° (the least favourable orientation for slip in these systems). On the other hand, the agreement of the corresponding second moments $\bar{\bar{\tau}}_{(1)}^{(r)}$ on these systems appears to be consistently predicted by the SC and FFT models. The main conclusion from these plots, however, is that the fluctuations in the hard systems are larger and increase in relative proportion as the nonlinearity increases, especially for the least favoured orientations for slip in these systems (near $\theta^{(r)} = 0$). The fluctuations in the soft systems are also seen to increase, although only slightly, for the least favoured orientations for these systems ($\theta^{(r)} = 90°$), but the predictions of the FFT and SC estimates are not completely consistent for the more favourable orientations of these systems (near $\theta^{(r)} = 0$). Thus, the FFT results suggest a slight increase of the fluctuations in the soft systems with increasing nonlinearity, while the SC estimates suggest a reduction. As pointed out by Liu & Ponte Castañeda (2003), this last result would be consistent with a more uniform state of stress developing on the soft systems, where the resolved shear stress would not be able to exceed its flow stress in the limit of ideally plastic behaviour. On the other hand, the average stresses in the hard systems are significantly below yield, suggesting that large fluctuations would be necessary to activate such systems, at least for some selected parts of the grains.

Figure 8 provides comparisons of the 'second-order' SC estimates (lines) and FFT results (symbols) for the average slip rates $\bar{\gamma}_{(1)}^{(r)}$ and $\bar{\gamma}_{(2)}^{(r)}$, as well as the corresponding second moments $\bar{\bar{\gamma}}_{(1)}^{(r)}$ and $\bar{\bar{\gamma}}_{(2)}^{(r)}$, plotted as functions of the grain orientation $\theta^{(r)}$. As in figure 7, the plots are for a fixed value of the grain anisotropy ($M = 9$) and correspond to several values of the nonlinearity ($n = 1, 3, 5, 10$, respectively). Again, the overall
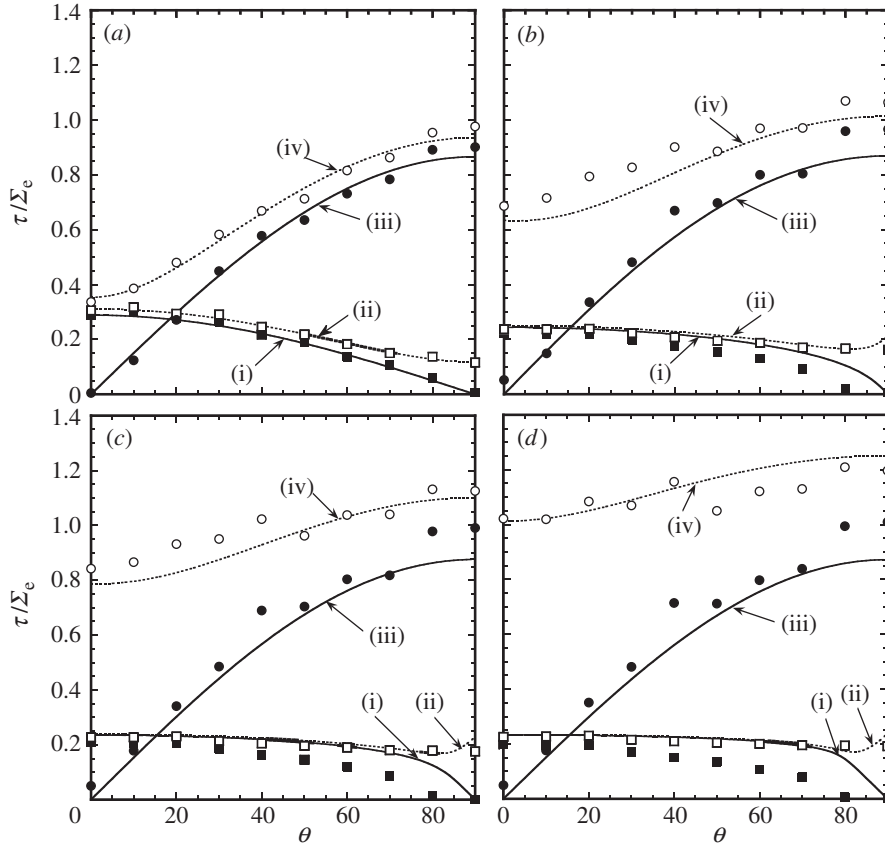
Figure 7. Comparison of the 'second-order' SC (lines) and FFT (symbols) estimates for the averages and second moments of the resolved shear stresses over grains with given orientation $\theta^{(r)}$ on the soft (1) and hard (2) slip systems, as functions of the grain orientation $\theta^{(r)}$, for grain anisotropy $M = 9$ and several values of the strain rate sensitivity $m = 1/n$: (a) $n = 1$, (b) $n = 3$, (c) $n = 5$ and (d) $n = 10$. The results are normalized by Σ_e. (i) $\bar{\tau}_{(1)}^{(r)}$; (ii) $\bar{\bar{\tau}}_{(1)}^{(r)}$; (iii) $|\bar{\tau}_{(2)}^{(r)}|$; (iv) $\bar{\bar{\tau}}_{(2)}^{(r)}$.

agreement is quite good, especially for low n, but the agreement is better this time for the soft systems. On the other hand, both the SC and FFT results appear to suggest that the average slip rates on the hard systems $\bar{\gamma}_{(2)}^{(r)}$ become progressively smaller with increasing values of n for all grain orientations, but the corresponding predictions for the second moments $\bar{\bar{\gamma}}_{(2)}^{(r)}$ seem to be inconsistent for lower values of $\theta^{(r)}$, where the FFT predictions are significantly larger than the SC estimates. Regardless of these localized differences, it may be seen that the slip rate fluctuations are much larger for the soft systems, especially for large values of n and for the least favoured orientation for these systems ($\theta^{(r)} = 90°$), where the average slip rate tends to zero. More generally speaking, even if the average slip rate on both systems can be seen to become very small with increasing nonlinearity for certain grain orientations, the fact that the fluctuations become quite large suggests that small sections of the grains would carry most of the deformation, which would be consistent with the shear band mechanism observed by Suquet (2001) for ideally plastic polycrystals.
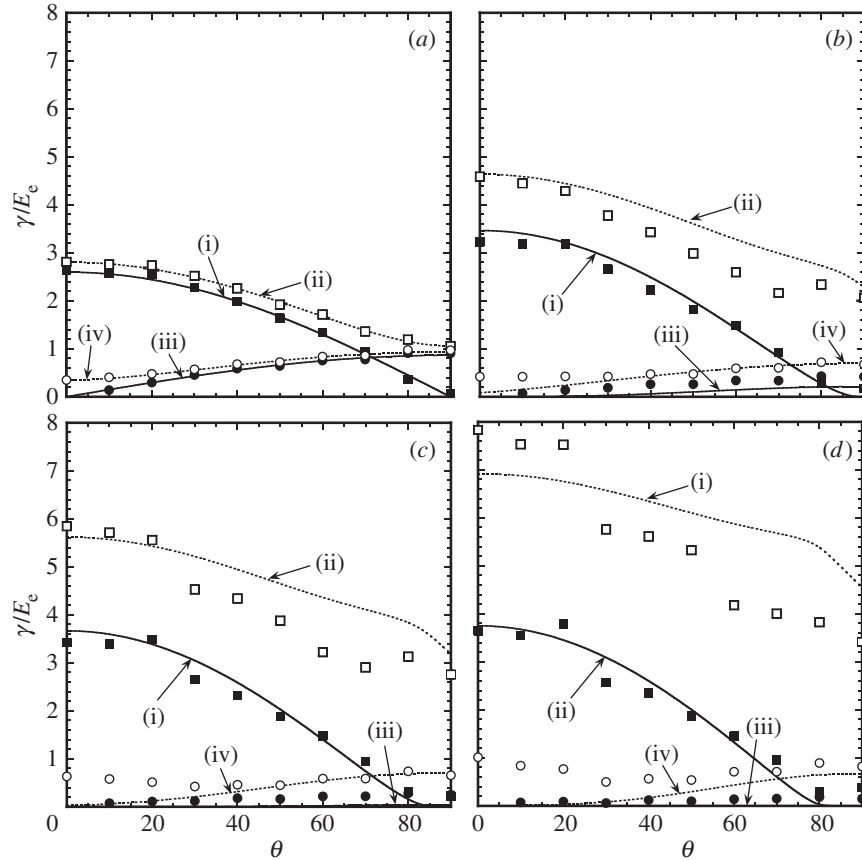
Figure 8. Comparison of the 'second-order' SC (lines) and FFT (symbols) estimates for the averages and second moments of the slip rates over grains with given orientation $\theta^{(r)}$ on the soft (1) and hard (2) slip systems, as functions of $\theta^{(r)}$, for grain anisotropy $M = 9$ and several values of the strain rate sensitivity $m = 1/n$: (a) $n = 1$, (b) $n = 3$, (c) $n = 5$, (d) $n = 10$. The results are normalized by E_e. (i) $\bar{\gamma}_{(1)}^{(r)}$; (ii) $\bar{\bar{\gamma}}_{(1)}^{(r)}$; (iii) $|\bar{\gamma}_{(2)}^{(r)}|$; (iv) $\bar{\bar{\gamma}}_{(2)}^{(r)}$.

5. Concluding remarks

In this paper, the FFT simulation technique and the 'second-order' homogenization method have been used to generate estimates for the effective behaviour of, as well as for the fluctuations of the stress and strain-rate fields in, model 2D power-law polycrystals with isotropic microstructures. Direct comparison of estimates obtained by means of both approaches required the calculation of ensemble averages of FFT solutions, over different random polycrystal configurations. In particular, for the linear case ($m = n = 1$), when the exact result is known (Dykhne 1970), it was found that the FFT simulations give accurate estimates for the effective behaviour. While it was also already known that the standard SC method reproduces exactly Dhykne's exact result for the effective behaviour of the linear 2D polycrystal, it was possible to check that the SC method also gives good (analytical) predictions for the fluctuations of the stress and strain-rate fields over the various grain orientations in

a linear polycrystal. In fact, the conjecture was made that the SC method should also reproduce exactly these higher-order statistical quantities for the polycrystal.

For nonlinear viscoplastic polycrystals, use of the SC approximation for the relevant 'linear comparison polycrystal' in the context of the 'second-order' homogenization method leads to estimates for the effective behaviour and field fluctuations that are in good overall agreement with the corresponding FFT results. More specifically, it was found that among the various extensions of the SC approximation for nonlinear viscoplastic polycrystals, including the 'incremental', 'variational' and 'tangent' extensions, the 'second-order' SC approximation was the *only one* capable of generating estimates for the effective behaviour that were consistent with the FFT simulations, especially for low rate sensitivities and high grain anisotropies (see figure 3). In addition, the 'second-order' SC predictions for the averages and fluctuations of the stress and strain-rate fields over the various grain orientations were found to be generally consistent with the corresponding FFT results, even if some localized differences were observed. Thus, both the overall stress and strain-rate fluctuations were found to increase with increasing grain anisotropy and decreasing strain-rate sensitivity, with the strain-rate fluctuations being generally larger than the corresponding stress fluctuations. That the fluctuations should increase with increasing grain anisotropy is consistent with the physics of the problem, which requires that certain components of the stress and strain tensors be continuous across grains with different orientations, leading to highly non-uniform fields within the grains. On the other hand, it follows from the 'second-order' approximation that nonlinear polycrystals can be thought of as 'linear' polycrystals with a grain anisotropy that scales as M^n, where M is the grain anisotropy of the nonlinear polycrystal and n is the nonlinearity exponent. It therefore also makes sense physically that the field fluctuations should increase with increasing nonlinearity.

Finally, it is noted that, while the results generated in this work are for a very special class of polycrystals, this class is expected to be highly representative of the behaviour of more general 3D classes of polycrystals. The fact that the 'second-order' SC estimates are quite accurate for the special class of 2D polycrystals is suggestive that they may also be quite accurate for more general 3D polycrystals. Work on 3D viscoplastic polycrystals is in progress and will be reported upon elsewhere.

References

Adams, B. L. & Olson, T. 1998 The mesostructure-properties linkage in polycrystals. *Prog. Mater. Sci.* **43**, 1–88.

Balasubramanian, S. & Anand, L. 2002 Plasticity of initially textured hexagonal polycrystals at high homologous temperatures: Application to titanium. *Acta Mater.* **50**, 133–148.

Beaudoin, A. J., Dawson, P. R., Mathur, K. K. & Kocks, U. F. 1995 A hybrid finite element formulation for polycrystal plasticity with consideration of macrostructural and microstructural linking. *Int. J. Plasticity* **11**, 501–521.

Bhattacharya, K. & Suquet, P. 2004 Transformation domains for a class of model polycrystals. (In preparation.)

deBotton, G. & Ponte Castañeda, P. 1995 Variational estimates for the creep behaviour of polycrystals. *Proc. R. Soc. Lond.* A **448**, 121–142.

Dykhne, A. M. 1970 Conductivity of a two-dimensional two-phase system. *Dokl. Akad. Nauk SSSR* **59**, 110–115.

Goldstein, G. H. 2001 Rigid perfectly plastic two-dimensional polycrystals. *Proc. R. Soc. Lond.* A **457**, 2789–2798.

Hershey, A. V. 1954 The elasticity of an isotropic aggregate of anisotropic cubic crystals. *ASME J. Appl. Mech.* **21**, 236–240.

Hill, R. 1965 Continuum micro-mechanics of elastoplastic polycrystals. *J. Mech. Phys. Solids* **13**, 89–101.

Hutchinson, J. W. 1976 Bounds and self-consistent estimates for creep of polycrystalline materials. *Proc. R. Soc. Lond.* A **348**, 101–127.

Kohn, R. V. & Little, T. D. 1998 Some model problems of polycrystal plasticity with deficient basic crystals. *SIAM J. Appl. Math.* **59**, 172–197.

Kröner, E. 1958 Berechnung der elastischen Konstanten des Vielkristalls aus den Konstanten des Einkristalls. *Z. Phys.* **151**, 504–518.

Kröner, E. 1986 Statistical modelling. In *Modelling small deformations of polycrystals* (ed. J. Gittus & J. Zarka), pp. 229–291. Elsevier.

Laws, N. 1973 On the thermostatics of composite materials. *J. Mech. Phys. Solids* **21**, 9–17.

Lebensohn, R. A. 2001 N-site modelling of a 3D viscoplastic polycrystal using the fast Fourier transform. *Acta Mater.* **49**, 2723–2737.

Lebensohn, R. A. & Tomé, C. N. 1993 A self-consistent anisotropic approach for the simulation of plastic deformation and texture development of polycrystals: application to zirconium alloys. *Acta Metall. Mater.* **41**, 2611–2624.

Lebensohn, R. A., Castelnau, O., Brenner, R. & Gilormini, P. 2004 Study of the antiplane deformation of linear 2-D polycrystals with different microstructures. (In the press.)

Liu, Y. & Ponte Castañeda, P. 2004 Second-order theory for the effective behavior and field fluctuations in viscoplastic polycrystals. *J. Mech. Phys. Solids* **52**, 467–495.

Masson, R., Bornert, M., Suquet, P. & Zaoui, A. 2000 An affine formulation for the prediction of the effective properties of nonlinear composites and polycrystals. *J. Mech. Phys. Solids* **48**, 1203–1227.

Michel, J., Moulinec, H. & Suquet, P. 1999 Effective properties of composite materials with periodic microstructure: a computational approach. *Comput. Meth. Appl. Mech. Engng* **172**, 109–143.

Michel, J., Moulinec, H. & Suquet, P. 2000 A computational method based on augmented Lagrangians and fast Fourier transforms for composites with high contrast. *Comp. Model. Engng Sci.* **1**, 79–88.

Molinari, A., Canova, G. R. & Ahzi, S. 1987 A self-consistent approach of the large deformation polycrystal viscoplasticity. *Acta Metall. Mater.* **35**, 2983–2994.

Moulinec, H. & Suquet, P. 1994 A fast numerical method for computing the linear and nonlinear properties of composites. *C. R. Acad. Sci. Paris Sér. II* **318**, 1417–1423.

Moulinec, H. & Suquet, P. 1998 A numerical method for computing the overall response of nonlinear composites with complex microstructure. *Comput. Meth. Appl. Mech. Engng* **157**, 69–94.

Nebozhyn, M. V., Gilormini, P. & Ponte Castañeda, P. 2001 Variational self-consistent estimates for cubic viscoplastic polycrystals: the effect of grain anisotropy and shape. *J. Mech. Phys. Solids* **49**, 313–340.

Nesi, V., Smyshlyaev, V. P. & Willis, J. R. 2000 Improved bounds for the yield stress of a model polycrystalline material. *J. Mech. Phys. Solids* **48**, 1799–1825.

Ponte Castañeda, P. 1991 The effective mechanical properties of nonlinear isotropic composites. *J. Mech. Phys. Solids* **39**, 45–71.

Ponte Castañeda, P. 1996 Exact second-order estimates for the effective mechanical properties of nonlinear composite materials. *J. Mech. Phys. Solids* **44**, 827–862.

Ponte Castañeda, P. 2002 Second-order homogenization estimates for nonlinear composites incorporating field fluctuations. I. Theory. *J. Mech. Phys. Solids* **50**, 737–757.

Ponte Castañeda, P. & Nebozhyn, M. 1997 Variational estimates of the self-consistent type for some model nonlinear polycrystals. *Proc. R. Soc. Lond.* A **453**, 2715–2724.

Ponte Castañeda, P. & Suquet, P. 1998 Nonlinear composites. *Adv. Appl. Mech.* **34**, 171–302.

Reuss, A. 1929 Berechnung der Fließgrenze von Mischkristallen auf Grund der Plastizitäts-bedingung für Einkristalle. *Z. Angew. Math. Mech.* **9**, 49–58.

Suquet, P. 2001 In *Proc. IUTAM Symp. on Computational Mechanics of Solid Materials at Large Strains, Stuttgart, Germany, 20–24 August 2001*.

Suquet, P. & Ponte Castañeda, P. 1993 Small-contrast perturbation expansions for the effective properties of nonlinear composites. *C. R. Acad. Sci. Paris Sér. II* **317**, 1515–1522.

Taylor, G. I. 1938 Plastic strains in metals. *J. Inst. Metals* **62**, 307–324.

Willis, J. R. 1977 Bounds and self-consistent estimates for the overall moduli of anisotropic composites. *J. Mech. Phys. Solids* **25**, 185–202.

Willis, J. R. 1981 Variational and related methods for the overall properties of composites. *Adv. Appl. Mech.* **21**, 1–78.